Relaxation Shortcuts through Boundary Coupling

Gianluca Teza, Ran Yaacoby, and Oren Raz

Phys. Rev. Lett. **131**, 017101 — Published 6 July 2023

DOI: 10.1103/PhysRevLett.131.017101

Relaxation shortcuts through boundary coupling

Gianluca Teza, Ran Yaacoby, and Oren Raz*
Department of Physics of Complex Systems, Weizmann Institute of Science, Rehovot 7610001, Israel
(Dated: April 12, 2023)

When a hot system cools down faster than an equivalent cold one, it exhibits the Mpemba Effect (ME). This counterintuitive phenomenon was observed in several systems including water, magnetic alloys and polymers. In most experiments the system is coupled to the bath through its boundaries, but all theories so far assumed bulk coupling. Here we build a general framework to characterize anomalous relaxations through boundary coupling, and present two emblematic setups: a diffusing particle and an Ising antiferromagnet. In the latter, we show that the ME can survive even arbitrarily weak couplings.

When coupled to a thermal bath, most systems relax towards equilibrium. While the equilibrium distribution is only a function of the system's Hamiltonian and temperature, the precise details of the relaxation are determined by many factors, including the intrinsic properties of the specific system, its initial condition, the bath's properties and the exact nature of the coupling between the system and the bath.

In the weak coupling limit, when the rate of heat exchange with the thermal environment is much slower than the energy relaxation within the system, it is generally expected that a macroscopic system initiated at equilibrium with temperature T_0 relaxes *quasi-statically* towards the bath temperature T_b, such that the system is in equilibrium for some temperature throughout the relaxation. This is a consequence of the self-thermalization generated by the energy diffusion within the system being much faster than the rate of heat exchange with the thermal bath. In strong couplings, however, the self-thermalization process that equilibrates the system is not fast enough, and the energy exchange with the environment drives the system into a relaxation trajectory that can reach far from any equilibrium distributions. Such far from equilibrium relaxation trajectories can be counterintuitive, and show interesting phenomena unexpected near equilibrium [1–5]. An important example is the Mpemba Effect (ME) [6, 7], where a hot system cools faster than an initially cold one when quenching both to an even colder bath. The ME was observed experimentally in a variety of setups, including water [8], magnetic alloys [9], polymers [10], clathrate hydrates [11] and very recently in small size systems like colloids diffusing in a potential [12–14]. It was also observed in a variety of numerical and theoretical models for water molecules [15–20], driven granular gases [21–26], inertial suspensions [27–29], gas of visco-elastic particles [30], diffusing in a potential [2, 31–34] and classical as well as quantum spin models [35–42].

The theoretical models proposed so far to explain anomalous relaxation phenomena as the ME used the simplifying assumption that all the relevant degrees of freedom (e.g. all spins or molecules) are directly coupled to the thermal bath. However, in all relevant experiments so far, only a small set out of the relevant degrees of freedom are coupled to the bath. For example, in water, clathrate hydrates and polymers, internal collisions between the molecules conserve energy, and the system exchanges heat with the bath only through boundary collisions [43, 44]. Even in the case of colloidal systems [12, 13], the colloid interacts with the liquid around them, but the liquid exchanges heat with the bath only through its boundaries.

In this letter, we construct a general theoretical framework for boundary coupling with the bath, and use it to demonstrate the existence of the ME even in such systems. We consider two types of systems: (i) systems where the relevant degrees of freedom (DoF) interact with a "local bath" composed of other degrees of freedom. In this case, the local temperature profile changes with a characteristic timescale, defining an interplay with the dynamics of the relevant DoF which will determine the possibility of observing ME and other anomalous relaxation phenomena. (ii) In systems where the same DoF play both the role of the relaxation and serves as a local bath, the situation is quite different: in these cases the ME is possible even in the arbitrarily weak coupling limit.

Diffusing particle. – A prominent example for the first kind of systems is a Brownian particle diffusing in a confining potential. When the system is quenched to some temperature, the fluid in which the particle is diffusing doesn't change its local temperature instantaneously and uniformly. Rather, its boundaries are coupled to a thermal bath, and the temperature profile changes according to some internal dynamics. If this dynamics is much faster than the particle diffusion, the liquid reaches its uniform temperature before the distribution of the relevant DoF (i.e. the position) changes in any way. This case coincides with the common assumption of instantaneous uniform quench in the temperature. In the opposite limit, the equilibration temperature profile is much slower than the diffusion, and the position of the particle follows the steady-state distribution associated with the instantaneous temperature profile. Anomalous relaxations can therefore exist only in the local bath temperature profile, which is assumed not to be the case. This

* oren.raz@weizmann.ac.il

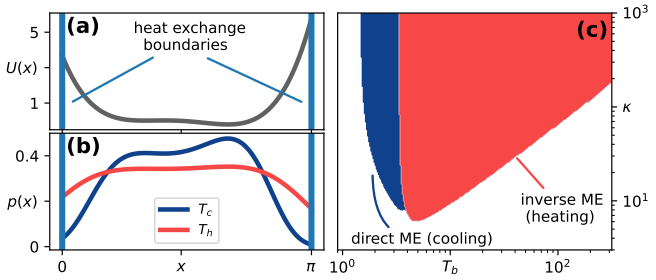

FIG. 1. (a) Double-well potential $U(x)$ similar to that used in colloidal experimental setups (see Refs. [12, 13]). (b) Examples of Boltzmann distributions at cold and hot bath temperatures for which the direct (cooling) and inverse (heating) ME exist. (c) Mpemba phase diagram as a function of the bath temperature T_b and thermal diffusivity κ.

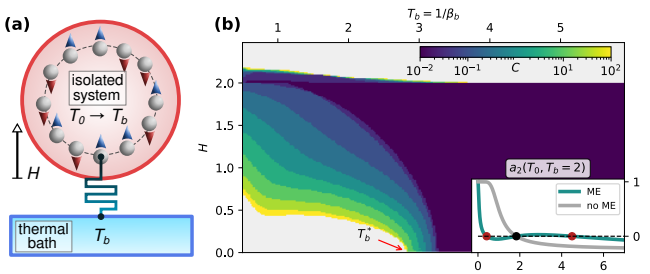

FIG. 2. (a) An antiferromagnet Ising chain, with a single spin coupled to the thermal bath. Transitions are allowed only if energy is conserved, except for flipping the spin coupled to the bath. (b) Minimal coupling strength C (colorbar) for which there exists some type of a ME at the corresponding bath temperature T_b (x axis) and H (y axis). In the white areas there is no ME at any coupling strength. Inset: the ME exists if $a_2(T_0, T_b)$ is nonmonotonic in T_0.

implies that a certain "critical coupling", determining the possibility of observing anomalous relaxation phenomena, exists.

To demonstrate this case, we use the Brownian particle in a potential used to demonstrate experimentally the inverse [13] and strong [12] Mpemba effects (see Fig. 1a). However, instead of using a uniform instantaneous quench of the temperature at all position as in [12, 13], here the system is coupled to the thermal bath only from its boundaries (Fig. 1a). We assume that the water's temperature profile follows the heat equation $\partial_t T(x,t) = \kappa \partial_x^2 T(x,t)$ with initial condition given by the spatially uniform initial temperature $T(x, t = 0) = T_0$ and thermal diffusivity κ. The probability density $p(x,t)$ of finding the particle in position x at some time t evolves according to the Fokker-Plank equation [45]:

$$\begin{aligned}\partial_t p(x,t) &= -\mu\partial_x\Big(\big(\partial_x U(x)\big)p(x,t)\Big) + \mu\partial_x^2\Big(T(x,t)p(x,t)\Big)\\ &\equiv \mathcal{L}(t)p(x,t) \end{aligned} \tag{1}$$

where $U(x)$ is the potential and μ is the mobility of the Brownian particle. The Fokker-Plank operator is time dependent, but in the long time limit $T(x) \to T_b$, implying $\mathcal{L}(t) \to \mathcal{L}_{T_b}$ which ensures convergence to the Boltzmann equilibrium $\pi_{T_b}(x) \propto e^{-U(x)/T_b}$ (we set $k_b = 1$). The eigenfunctions of $\mathcal{L}_{T_b}$, solving $\mathcal{L}_{T_b} v_i(x, T_b) = \lambda_i v_i(x, T_b)$ with $0 = \lambda_1 > \lambda_2 \geq \lambda_3 \geq \ldots$, form a complete basis, therefore:

$$p(x,t) = \pi_{T_b}(x) + \sum_{i>1} a_i(T_0, T_b, t) e^{\lambda_i(T_b)t} v_i(x, T_b) \tag{2}$$

where $a_i(t)$ is a coefficient retaining information on the initial conditions of the system, as well as the temperature profile.

In the limit of an instantaneous quench, a_i are time independent, and a_2 encodes the existence of the ME, as was used in [12, 13]: a nonmonotonic dependence in T_0 implies the existence of a relaxation shortcut when quenching the system to T_b, which can be exponentially faster if $a_2 = 0$ for some initial condition (a *strong* ME).

However, when the timescale of the quench is comparable to that of the diffusing particle, one cannot rely on the same analysis as in [12, 13], as a_2 has a nonexponential time dependence due to the time-dependent temperature profile. In the last stages of the relaxation, one can nevertheless approximate the difference from equilibrium $\Delta p(x,t) = p(x,t) - \pi_{T_b}(x) \simeq a(t)v_2(x)$ for some $a(t)$ decaying exponentially fast. Identifying a sign change in $a(t)$ is therefore enough to ensure the existence of a strong ME. Formally, this can be done through the Mpemba parity index [40]

$$I^{\pm}(t, T_b) = \mathrm{sgn} \int dx\ \Delta p^{\pm}(x,t) \Delta p^{\pm\delta T}(x,t) \tag{3}$$

where the differences $\Delta p^{\pm}$ refer to quenches to T_b starting from initial temperatures $T_0 = \{+\infty, 0\}$, while $\Delta p^{\pm\delta T}$ to quenches starting from $T_0 = T_b \pm \delta T$, for some $\delta T > 0$. A negative sign of I^+ (I^-) in the long time limit implies that for some $T > T_b$ ($T < T_b$) the coefficient $a_2 \equiv 0$, ensuring the existence of a strong direct (inverse) ME. For the given potential $U(x)$ (Fig. 1a), and for each set of T_b and κ, it is possible to evaluate numerically $I^{\pm}$ as demonstrated in Fig. 1c. As expected, for a given value of T_b, there exists a critical value of κ below which the ME cannot be observed.

Boundary DoF coupling. – Let us next discuss a different type of systems, in which all the DoF are modeled, but only the boundary DoF can exchange heat with the environment. For simplicity, we use a discrete state systems with probability distribution $\vec{p}(t)$ where the component $p_i(t)$ is the probability to be in a microstate i at a given time t. $\vec{p}(t)$ evolves in time according to a Markovian master equation

$$\partial_t \vec{p}(t) = \mathbf{W}(T_b)\vec{p}(t), \tag{4}$$

where the rate matrix $\mathbf{W}$ generalizes the Fokker-Plank operator $\mathcal{L}$ and encodes the specific model. The off-diagonal terms $\mathbf{W}_{ij}$ are the transition rates from state

j to state i, while the diagonal term $\mathbf{W}_{ii} = -\sum_{j\neq i}\mathbf{W}_{ji}$ represents the escape rate from the state i. We assume that detailed balance and ergodicity hold, so that regardless of the initial condition the system relaxes towards the Boltzmann distribution $\pi_i(T_b) \propto e^{-E_i/T_b}$ where E_i is the energy of the microstate i. In this case, the relaxation process from equilibrium with an initial temperature T_0 is a discrete analogue of Eq. 2, allowing us to straightforwardly characterize the ME through the coefficient a_2 [1]. For simplicity, in what follows, we do not distinguish between different types of the ME.

To model the common scenario where heat can be transferred only through DoF sitting on the boundaries, we first distinguish between "boundary transitions" of boundary DoF that can exchange heat with the bath, and "bulk transitions" in which no energy is exchanged with the bath and they can only happen between same-energy states. Bulk transitions serve as a *self-thermalization* (ST) mechanism, whereas the boundary transitions generate *bath coupling* (BC) and enable transitions between different energy shells. This structure can be modeled by

$$\mathbf{W}(\Gamma^{ST},\Gamma^{BC}) = \Gamma^{ST}\mathbf{W}^{ST} + \Gamma^{BC}\mathbf{W}^{BC}. \tag{5}$$

Here $\mathbf{W}^{ST}$ and $\mathbf{W}^{BC}$ are normalized rate matrices corresponding to the self thermalization and boundary coupling transitions respectively, and $\Gamma^{\{ST,BC\}}$ are coupling constants modulating the rates amplitude. Their ratio, $C = \Gamma^{BC}/\Gamma^{ST}$, dictates the coupling strength [46]: in the limit $C \ll 1$ boundary flips occur rarely compared to thermalization flips, hence the system thermalizes quickly after each heat exchange with the bath. In the $C \gg 1$ limit, the boundaries exchange heat much faster than the thermalization and the diffusion of energy within the system sets the timescale for the relaxation. We refer to the former limit as *weak coupling* and to the latter as *strong coupling*. By construction, $\mathbf{W}^{BC}$ is generally sparse and $\mathbf{W}^{ST}$ contains only transitions between same-energy states, implying a degeneracy of its zeroth eigenvalue equivalent to the number of energy shells.

In the weak coupling limit, a naive perturbation scheme with $C \ll 1$ would not prove useful: for $C = 0$ the matrix $\mathbf{W}$ is reducible and its zero eigenvalue is highly degenerate, so one cannot apply the standard analysis. Instead, it is constructive in this case to aggregate all the microstates that share the same energy into a single *macrostate* and construct the effective dynamics by summing all the microscopic transitions between them [47, 48]. The dynamics is then dictated only by the boundary flips, and the diffusion within each energy shell is assumed to happen instantaneously. Similarly, in the strong coupling limit, micro-states can be aggregated into macrostates by combining all the microstates connected by boundary flips. Mathematically, the two aggregation procedures can be done by arranging the states such that $\mathbf{W}^{BC}$ or $\mathbf{W}^{ST}$ is block diagonal where each block corresponds to transitions within a macrostate, and coarsening over these blocks.

Ising antiferromagnet. – Let us demonstrate the above construction with a specific example of N Ising spins on a ring, with nearest neighbour antiferromagnet interactions (Fig. 2a). Each spin $\{\sigma_s\}_{s=1\ldots N}$ can either be in a $+1$ or -1 state, giving a total of $M = 2^N$ different microstates, identified by $\vec{\sigma} = (\sigma_1, ..., \sigma_N)$. The Hamiltonian of the system is

$$\mathcal{H}(\vec{\sigma}) = -J\sum_s \sigma_s\sigma_{s+1} - H\sum_{s=1}^{N}\sigma_s, \tag{6}$$

where $J < 0$ is the coupling constant, H is an external magnetic field and $\sigma_{N+1} \equiv \sigma_1$. For simplicity, we set $J = -1$.

As a boundary, we choose a specific spin (say σ_1) to be coupled to the bath. This implies that a general microstate $\vec{\sigma}$ is connected through thermal flips only with a single state $\vec{\sigma}'$ in which the first spin is flipped, $\sigma_1 \to -\sigma_1$, while the remaining spins are unaltered. The transition between two general microstates $\vec{\sigma}^{\{i,j\}}$ is therefore

$$\mathbf{W}^{BC}_{ij} = \frac{\delta_{\sigma_1^i,-\sigma_1^j}\prod_{s>1}\delta_{\sigma_s^i,\sigma_s^j}}{1+e^{(\mathcal{H}(\vec{\sigma}^i)-\mathcal{H}(\vec{\sigma}^j))/T_b}} \tag{7}$$

where δ_{ij} is the Kronecker delta, σ_s^i is the s spin in the microstate $\vec{\sigma}^i$ and we used standard Glauber dynamics as the transition weight [49, 50], ensuring equilibration to a Boltzmann distribution.

To model bulk transitions we use rates that decay exponentially as $2^{-d_{ij}}$, where $d_{ij} = \sum_s \delta_{\sigma_s^i,-\sigma_s^j}$ is the Hamming distance [51] that counts the number of spins that has to be flipped between the two configurations. Alternative metrics that keep into account space locality (e.g. the generalized Hamming distance [52]) could be implemented. While for weak couplings the specific details of d_{ij} become irrelevant, for strong couplings locality constraints limit the connectivity within an energy shell, effectively enhancing the out-of-equilibrium character of the relaxation process (see SM [53]). We therefore formalize bulk transitions between two states $i \neq j$ as

$$\mathbf{W}^{ST}_{ij} = \delta_{\mathcal{H}(\vec{\sigma}^i),\mathcal{H}(\vec{\sigma}^j)}2^{-d_{ij}}. \tag{8}$$

The full transition matrix for the model is built as a linear combination of the two rate matrices as in Eq. 5.

Let us consider the persistence of the ME in this setup. In Fig. 2b we plot for each T and H the minimal coupling constant C for which some type of a ME exists in the system, for $N = 10$. The strength of the coupling affects only *quantitatively* the regions where the ME can be observed (the larger C, the larger the area). In particular, for any $|H| \leq 2$ the effect exists for any $T > T_b^*$, highlighted in Fig. 2b with a red arrow.

In the weak coupling case ($C \ll 1$), the coarse-grained rate matrix is given by

$$\mathbf{W}^{\text{weak}}_{ij} = \frac{G_{ij}}{\Omega_j}\frac{1}{1+e^{(E_i-E_j)/T_b}} \tag{9}$$

where the indices i, j now refer to the energies E_i and E_j, the (symmetric) matrix G_{ij} counts the number of transitions connecting microstates in the two energy shells, and

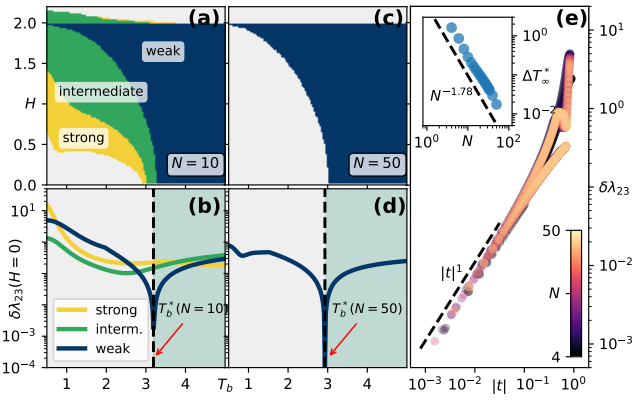

FIG. 3. (a) Comparison of the ME for different coupling strengths ($N = 10$). The strong coupling limit ($C \gg 1$) includes all colored areas, while the intermediate coupling ($C = 1$) is limited to the green and blue ones. Surprisingly, the effect survives the arbitrarily weak coupling limit ($C \ll 1$, blue area). (b) Distance between the second and third eigenvalues $\delta\lambda_{23}$ as a function of T_b for $H = 0$. A crossing of the eigenvalues clearly marks the beginning of the Mpemba region at T_b^* for the weakly coupled model. (c,d) Phase diagram in the weak coupling limit for $N = 50$. (e) Collapse of $\delta\lambda_{23}$ for different sizes show a dependence on the rescaled temperature $\propto |t|^1$. In the inset, the distance from the asymptotic $T_b^* \sim 2.91$ scales superlinearly.

Ω_i is the number of microstates with energy E_i. This coarsening considerably reduces the size of the matrix, allowing to numerically analyze longer chains assessing the stability of the phase diagram in the thermodynamic limit. The total number of energy shells in this case grows only quadratically as $2 + (N/2)^2$, as opposed to the exponential growth of the number of microstates. As an example, at $N = 50$ (Fig. 3c,d) there are $\sim 10^{15}$ microstates, but only 627 macrostates in the coarse-grained representation. A specific example exhibiting a strong ME in this setup is presented in the SM [53].

Extremely strong couplings ($C \gg 1$) can be similarly analyzed. In our model only a single spin is coupled to the bath, therefore the clustering of a N spins chain model results in an effective $N-1$ long chain with an additional "superposed" spin oscillating infinitely fast between the two ± 1 states. Indicating with i one of the possible 2^{N-1} configurations of the bulk chain, we set $\mathcal{H}_i^{\pm 1}$ to be the Hamiltonians of each of the two possible states in the i-th cluster. The two states composing a cluster are not equivalent as in the weak coupling case. To correctly define the transition rates in the coarse-grained model we therefore need to introduce a Glauber weight: $w_j^\sigma = e^{-\mathcal{H}_j^\sigma/T_b}/(e^{-\mathcal{H}_j^{-1}/T_b} + e^{-\mathcal{H}_j^{+1}/T_b})$ with $\sigma = \pm 1$ depending on the microstate from which the original transition occurred. This provides us with:

$$\mathbf{W}_{ij}^{\text{strong}} = \sum_{\sigma,\sigma'} w_j^\sigma \delta_{\mathcal{H}_j^\sigma, \mathcal{H}_i^{\sigma'}} 2^{-(d_{ij} + \delta_{\sigma,-\sigma'})} \tag{10}$$

where the Kroneker delta corrects the Hamming distance for the coupled spin. The area in which an effect can be observed is wider (Fig. 3a): a stronger coupling should indeed ease the undertake of anomalous relaxation paths.

In Fig. 3(a) we plot the regions in which some ME can be observed in the limiting coupling setups discussed above, and compare them with the intermediate $C = 1$ case. Surprisingly, the ME can be observed even for $C \ll 1$, demonstrating that the effect survives the limit of arbitrarily weak coupling. This counterintuitive result is related to the discrete nature of the DoF of the system [54]. Indeed, Glauber dynamics (Eq. 7) allows transitions only among configurations that differ by a single spin flip. This implies that energy shells with a microscopic energy difference (namely $\Delta E \sim 1$ even though $E \sim N$) might still be very far in terms of transitions. As a result, the self thermalization process has the same characteristic timescale as that of the boundary transitions. Therefore for arbitrarily weak couplings, even in the thermodynamic limit the system is forced to explore out-of-equilibrium configurations that allow the existence of anomalous relaxation effects (i.e. the ME). The colloidal particle setup (Fig. 1) provides a counter-example in which the continuous DoF break such mechanisms, setting a minimal value of the coupling strength below which no ME can be observed.

The boundary coupling setup we introduced offers a straightforward implementation for multiple baths coupling. If the baths are set at different temperatures, the rate matrix no longer abides by detailed balance, driving the system towards a nonequilibrium steady-state (NESS) that does not correspond to any Boltzmann distribution [48, 55, 56]. Non-dominant eigenvalues can be complex-valued, determining the onset of oscillating relaxations [53] where an analogous ME analysis allows to determine which initial equilibrium conditions relax the fastest (or slowest) to the NESS.

Finally, our analysis highlights a strong connection between the ME and the phenomenon of *eigenvalue crossing* of the transition matrix $\mathbf{W}$ with respect to the bath temperature T_b [57], which was recently connected to a new kind of dynamical phase transitions that further consolidates the parallel between singularities in the dynamics and equilibrium phase transitions [58–60]. In weakly coupled systems, an analysis of at $\delta\lambda_{23} = (\lambda_3 - \lambda_2)/\lambda_2$ at $H = 0$ shows how the bath temperature above which the ME can be observed is determined by a crossing at a certain "critical" temperature T_b^*. This corresponds to a singularity in the eigenvector regulating the direction of the slowest relaxation, determining the conditions that allow the existence of the ME (Fig. 3b,d). Analyses at different sizes show an excellent multi-scale collapse [61] on the rescaled temperature $t = (T_b - T_b^*)/T_b^*$ around zero, with a dependence $\delta\lambda_{23} \propto |t|^1$ (Fig. 3e). The critical temperature at finite sizes approaches the asymptotic value $T_b^* \sim 2.91$ with a superlinear decay (inset), ensuring that the analysis at $N = 50$ is consistent with the thermodynamic limit. With respect to setups in higher dimensions, a 2D squared lattice with a side of N spins

has a surface to volume ratio $4N/N^2 = 4/N$, while for a 3D cubic lattice the ratio is $6N^2/N^3 = 6/N$. Therefore, the 1D case we addressed with a ratio $1/N$ represents the most pronounced scenario. The ratio is of the same order independently of the dimension ($\sim N^{-1}$), suggesting that the same phenomenology should be observed in higher-dimensional setups.

Remarks. – We constructed a theoretical framework to characterize the evolution of a system coupled to the thermal bath only through its boundaries, presenting two complementary emblematic models with continuous and discrete DoF, respectively. While in the former a minimal intensity for the coupling is required, in the latter we proved how anomalous relaxation effects can survive arbitrary weak couplings. The proposed framework is general and applicable to any memoryless system exchanging heath with the thermal bath through limited DoF, including relaxations towards NESS [53]. Our results corroborate the validity of the ME as an nonequilibrium phenomenon, proving it is not an artifact due to full couplings. Far from equilibrium relaxations in the weak coupling limit are yet another counterintuitive result related to the discreteness of the DoF [54].

ACKNOWLEDGMENTS

O. R. is the incumbent of the Shlomo and Michla Tomarin career development chair, and is supported by the Abramson Family Center for Young Scientists, the Israel Science Foundation Grant No. 950/19 and by the Minerva foundation. G. T. is supported by the Center for Statistical Mechanics at the Weizmann Institute of Science, the grant 662962 of the Simons foundation, the grants HALT and Hydrotronics of the EU Horizon 2020 program and the NSF-BSF grant 2020765. We thank David Mukamel and Attilio L. Stella for useful discussions.

[1] Z. Lu and O. Raz, Nonequilibrium thermodynamics of the Markovian Mpemba effect and its inverse, Proceedings of the National Academy of Sciences of the United States of America 10.1073/pnas.1701264114 (2017).
[2] A. Gal and O. Raz, Precooling Strategy Allows Exponentially Faster Heating, Physical Review Letters 10.1103/PhysRevLett.124.060602 (2020).
[3] A. Lapolla and A. c. v. Godec, Faster uphill relaxation in thermodynamically equidistant temperature quenches, Phys. Rev. Lett. **125**, 110602 (2020).
[4] A. Militaru, A. Lasanta, M. Frimmer, L. L. Bonilla, L. Novotny, and R. A. Rica, Kovacs memory effect with an optically levitated nanoparticle, Phys. Rev. Lett. **127**, 130603 (2021).
[5] R. Holtzman and O. Raz, Landau theory for the mpemba effect through phase transitions, Communications Physics **5**, 280 (2022).
[6] Aristotle, *Meteorology* (Harvard University Press).
[7] E. B. Mpemba and D. G. Osborne, Cool?, Physics Education **4**, 172 (1969).
[8] M. Jeng, The Mpemba effect: When can hot water freeze faster than cold?, American Journal of Physics 10.1119/1.2186331 (2006).
[9] P. Chaddah, S. Dash, K. Kumar, and A. Banerjee, Overtaking while approaching equilibrium, arXiv preprint arXiv:1011.3598 (2010).
[10] C. Hu, J. Li, S. Huang, H. Li, C. Luo, J. Chen, S. Jiang, and L. An, Conformation directed mpeMba effect on polylactide crystallization, Crystal Growth and Design 10.1021/acs.cgd.8b01250 (2018).
[11] Y.-H. Ahn, H. Kang, D.-Y. Koh, and H. Lee, Experimental verifications of mpemba-like behaviors of clathrate hydrates, Korean Journal of Chemical Engineering , 1 (2016).
[12] A. Kumar and J. Bechhoefer, Exponentially faster cooling in a colloidal system, Nature 10.1038/s41586-020-2560-x (2020), arXiv:2008.02373.
[13] A. Kumar, R. Chétrite, and J. Bechhoefer, Anomalous heating in a colloidal system, Proceedings of the National Academy of Sciences **119** (2022).
[14] J. Bechhoefer, A. Kumar, and R. Chétrite, A fresh understanding of the mpemba effect, Nature Reviews Physics **3**, 534 (2021).
[15] Y. Tao, W. Zou, J. Jia, W. Li, and D. Cremer, Different Ways of Hydrogen Bonding in Water - Why Does Warm Water Freeze Faster than Cold Water?, Journal of Chemical Theory and Computation **13**, 55 (2016).
[16] X. Zhang, Y. Huang, Z. Ma, Y. Zhou, J. Zhou, W. Zheng, Q. Jiang, and C. Q. Sun, Hydrogen-bond memory and water-skin supersolidity resolving the Mpemba paradox, Physical Chemistry Chemical Physics **16**, 22995 (2014).
[17] M. Vynnycky and S. Kimura, Can natural convection alone explain the Mpemba effect?, International Journal of Heat and Mass Transfer **80**, 243 (2015).
[18] D. Auerbach, Supercooling and the Mpemba effect: When hot water freezes quicker than cold, American Journal of Physics **63**, 882 (1998).
[19] S. M. Mirabedin and F. Farhadi, Numerical investigation of solidification of single droplets with and without evaporation mechanism, International Journal of Refrigeration **73**, 219 (2017).
[20] A. Gijón, A. Lasanta, and E. R. Hernández, Paths towards equilibrium in molecular systems: The case of water, Phys. Rev. E **100**, 032103 (2019).
[21] A. Lasanta, F. Vega Reyes, A. Prados, and A. Santos, When the Hotter Cools More Quickly: Mpemba Effect in Granular Fluids, Physical Review Letters 10.1103/PhysRevLett.119.148001 (2017), arXiv:1611.04948.
[22] A. Torrente, M. A. López-Castaño, A. Lasanta, F. V. Reyes, A. Prados, and A. Santos, Large mpemba-like effect in a gas of inelastic rough hard spheres, Physical Review E **99**, 060901 (2019).
[23] A. Biswas, V. Prasad, O. Raz, and R. Rajesh, Mpemba effect in driven granular maxwell gases, Physical Review E **102**, 012906 (2020).
[24] A. Santos and A. Prados, Mpemba effect in molecular

gases under nonlinear drag, Physics of Fluids **32**, 072010 (2020).
[25] A. Biswas, V. V. Prasad, and R. Rajesh, Mpemba effect in anisotropically driven inelastic maxwell gases, Journal of Statistical Physics **186**, 45 (2022).
[26] A. Megías, A. Santos, and A. Prados, Thermal versus entropic mpemba effect in molecular gases with nonlinear drag, arXiv preprint arXiv:2201.13130 (2022).
[27] S. Takada, H. Hayakawa, and A. Santos, Mpemba effect in inertial suspensions, Physical Review E **103**, 032901 (2021).
[28] R. Gómez González, N. Khalil, and V. Garzó, Mpemba-like effect in driven binary mixtures, Physics of Fluids **33**, 053301 (2021).
[29] R. G. González and V. Garzó, Non-monotonic mpemba effect in binary molecular suspensions, in *EPJ Web of Conferences*, Vol. 249 (EDP Sciences, 2021) p. 09005.
[30] E. Mompó, M. López-Castaño, A. Lasanta, F. Vega Reyes, and A. Torrente, Memory effects in a gas of viscoelastic particles, Physics of Fluids **33**, 062005 (2021).
[31] R. Chétrite, A. Kumar, and J. Bechhoefer, The metastable mpemba effect corresponds to a non-monotonic temperature dependence of extractable work, Frontiers in Physics **9**, 141 (2021).
[32] M. R. Walker and M. Vucelja, Anomalous thermal relaxation of langevin particles in a piecewise-constant potential, Journal of Statistical Mechanics: Theory and Experiment **2021**, 113105 (2021).
[33] D. M. Busiello, D. Gupta, and A. Maritan, Inducing and optimizing markovian mpemba effect with stochastic reset, New Journal of Physics **23**, 103012 (2021).
[34] F. J. Schwarzendahl and H. Löwen, Anomalous cooling and overcooling of active systems, arXiv preprint arXiv:2111.06109 10.48550/arXiv.2111.06109 (2021).
[35] F. Carollo, A. Lasanta, and I. Lesanovsky, Exponentially accelerated approach to stationarity in markovian open quantum systems through the mpemba effect, Phys. Rev. Lett. **127**, 060401 (2021).
[36] M. Baity-Jesi, E. Calore, A. Cruz, L. A. Fernandez, J. M. Gil-Narvión, A. Gordillo-Guerrero, D. Iñiguez, A. Lasanta, A. Maiorano, E. Marinari, *et al.*, The mpemba effect in spin glasses is a persistent memory effect, Proceedings of the National Academy of Sciences **116**, 15350 (2019).
[37] A. Nava and M. Fabrizio, Lindblad dissipative dynamics in the presence of phase coexistence, Physical Review B **100**, 125102 (2019).
[38] Z.-Y. Yang and J.-X. Hou, Non-markovian mpemba effect in mean-field systems, Physical Review E **101**, 052106 (2020).
[39] N. Vadakkayil and S. K. Das, Should a hotter paramagnet transform quicker to a ferromagnet? monte carlo simulation results for ising model, Physical Chemistry Chemical Physics **23**, 11186 (2021).
[40] I. Klich, O. Raz, O. Hirschberg, and M. Vucelja, Mpemba Index and Anomalous Relaxation, Physical Review X 10.1103/PhysRevX.9.021060 (2019), arXiv:1711.05829.
[41] I. González-Adalid Pemartín, E. Mompó, A. Lasanta, V. Martín-Mayor, and J. Salas, Slow growth of magnetic domains helps fast evolution routes for out-of-equilibrium dynamics, Phys. Rev. E **104**, 044114 (2021).
[42] Z.-Y. Yang and J.-X. Hou, Mpemba effect of a mean-field system: The phase transition time, Physical Review E **105**, 014119 (2022).
[43] R. Tehver, F. Toigo, J. Koplik, and J. R. Banavar, Thermal walls in computer simulations, Physical Review E **57**, R17 (1998).
[44] D. Toton, C. D. Lorenz, N. Rompotis, N. Martsinovich, and L. Kantorovich, Temperature control in molecular dynamic simulations of non-equilibrium processes, Journal of Physics: Condensed Matter **22**, 074205 (2010).
[45] N. Van Kampen, Diffusion in inhomogeneous media, Journal of physics and chemistry of solids **49**, 673 (1988).
[46] The specific normalization chosen for $\mathbf{W}^{\{BC,ST\}}$ changes the value of C, but not its limiting cases. Specifically, we chose to normalize with respect to the maximum rate so that $\max(\mathbf{W}^{ST}_{ij}) = \max(\mathbf{W}^{BC}_{ij}) \equiv 1$.
[47] G. Teza and A. L. Stella, Exact coarse graining preserves entropy production out of equilibrium, Phys. Rev. Lett. **125**, 110601 (2020).
[48] G. Teza, *Out of equilibrium dynamics: from an entropy of the growth to the growth of entropy production*, Ph.D. thesis, University of Padova (2020).
[49] R. J. Glauber, Time-dependent statistics of the Ising model, Journal of Mathematical Physics **4**, 294 (1963).
[50] B. U. Felderhof, Spin relaxation of the Ising chain, Reports on Mathematical Physics **1**, 215 (1971).
[51] R. W. Hamming, Error Detecting and Error Correcting Codes, Bell System Technical Journal **29**, 147 (1950).
[52] A. Bookstein, V. A. Kulyukin, and T. Raita, Generalized hamming distance, Information Retrieval **5**, 353 (2002).
[53] See supplemental material at ... for additional details of the calculations at the basis of the results presented in the main text.
[54] G. Teza, R. Yaacoby, and O. Raz, Far from equilibrium relaxation in the weak coupling limit, arXiv preprint arXiv:2203.11644 10.48550/arXiv.2203.11644 (2022).
[55] S. Katz, J. L. Lebowitz, and H. Spohn, Phase transitions in stationary nonequilibrium states of model lattice systems, Phys. Rev. B **28**, 1655 (1983).
[56] G. Teza, S. Iubini, M. Baiesi, A. L. Stella, and C. Vanderzande, Rate dependence of current and fluctuations in jump models with negative differential mobility, Physica A: Statistical Mechanics and its Applications **552**, 123176 (2020), tributes of Non-equilibrium Statistical Physics.
[57] G. Teza, R. Yaacoby, and O. Raz, Eigenvalue crossing as a phase transition in relaxation dynamics, arXiv preprint arXiv:2209.09307 10.48550/arXiv.2209.09307 (2022).
[58] A. L. Stella, A. Chechkin, and G. Teza, Anomalous dynamical scaling determines universal critical singularities, arXiv preprint arXiv:2209.02042 10.48550/arXiv.2209.02042 (2022).
[59] A. L. Stella, A. Chechkin, and G. Teza, Universal singularities of anomalous diffusion in the richardson class, arXiv preprint arXiv:2211.14878 10.48550/arXiv.2211.14878 (2022).
[60] J. Meibohm and M. Esposito, Finite-time dynamical phase transition in nonequilibrium relaxation, Phys. Rev. Lett. **128**, 110603 (2022).
[61] G. Teza, S. Suweis, M. Gherardi, A. Maritan, and M. Cosentino Lagomarsino, Network model of conviction-driven social segregation, Phys. Rev. E **99**, 032310 (2019).